Idealized Model for Plasma Acceleration in an MHD Channel

K. Kuriki,* Y. Kunii,† and Y. Shimizu‡
Institute of Space and Astronautical Science, Tokyo, Japan

A quasi-one-dimensional plasma acceleration by a self-induced magnetic field was analyzed in the magnetohydrodynamic framework. The magnetic Reynolds number was a similar parameter to describe the fields of flow and discharge current. The discharge current was found to be concentrated not only at the exit but also the entrance of the channel. By suitable electrode geometry, the current concentration was relaxed and the thrust efficiency was enhanced compared with the straight geometry.

Introduction

THE present MHD analysis has been motivated by the current concentration problem of the MPD arcjet. It has been found experimentally in our thruster models,[1] although not reported explicitly in the reference, that severe erosion occurs on the cathode surfaces near the tip and base at large discharge current and small propellant flow rate as shown in Fig. 1. There are several conceivable causes that explain the current concentration: 1) the initial breakdown of injected neutral gas, 2) the surface breakdown on the base insulator surface, and 3) the magnetohydrodynamic effect inherent in the plasma acceleration. The present study proposes to investigate the possibility of the third cause. It has been conceived intuitively that the current concentration at the cathode tip or the accelerator exit results from the blowout of the discharge current. The current concentration near the base or inlet, on the other hand, is rather contradictory to the blowout concept, and requires more rigorous treatment.

Seals and Hassan[2] made an analysis on the plasma acceleration in the discharge chamber of MPD arcjet. In their analysis various effects, such as nonequilibrium ionization, magnetohydrodynamics, Hall effect, and electrode geometry, are all taken into account. This model is realistic, but too complicated to find the key parameter influencing the current distribution. Hügel et al.[3] analyzed the flow in a self-field MPD arcjet. It is assumed in their analysis that the cathode current flows only in its front surface and the magnetic Reynolds number Rm is smaller than unity. The former assumption is inadequate to discuss the current concentration near the cathode base, and the latter ignores $J^2/\dot{m}$ dependence which is included in Rm. Here J and $\dot{m}$ represent the discharge current and the mass flow rate, respectively. Kimura et al.[4] studied the current distribution in a self-field MPD arcjet. They took into account the Hall effect and assume the magnetic Reynolds number to be small. Although the current concentration is found at the cathode tip and base, the concentration at the tip does not result from the current blowout but mainly from the geometrical effect. The concentration at the base results from the Hall effect.

In the present study, the nonlinear MHD flow is analyzed for a simple configuration, i.e., the quasi-one-dimensional channel flow. The Hall effect is ignored. Our approach to find the parametric dependence of MPD arcjet characteristics is to emphasize one particular effect and to construct the design guidelines step by step. Objectives of the present study are 1) to find a key parameter influencing the current concentration, 2) to find how the electrode geometry affects the current distribution and the thrust efficiency, and 3) to find how the physical dimension affects the acceleration characteristics, i.e., the scaling law.

Presented as Paper 81-0685 at the AIAA/JSASS/DGLR 15th International Electric Propulsion Conference, Las Vegas, Nev., April 21-23, 1981; submitted April 30, 1981; revision received March 22, 1982.

*Professor. Member AIAA.
†Graduate Student of University of Tokyo.
‡Research Engineer.

Formulation

The present analysis has been made in the magnetohydrodynamic framework under the following assumptions: 1) the flow is steady and quasi-one-dimensional with variable electrode separation; 2) the Hall effect is ignored; 3) the ionization processes are ignored; 4) the electromagnetic acceleration is more important than the aerodynamic one; 5) the electrical conductivity σ and the permeability μ are uniform and constant; and 6) the velocity at the inlet of the accelerator is zero.

The first assumption is applicable to the axisymmetric accelerator if the separation is smaller than the transverse radius of curvature and gradually changes in the axial direction. The second assumption is made to simplify the analysis. Under this assumption the streamwise component of the discharge current and the radial plasma motion are ignored. The third assumption concerns the gas breakdown and further ionization near the neutral gas inlet. Under this assumption it remains unsolved whether the gas breakdown is a possible cause of the current concentration. The fourth assumption is valid in the plasma accelerator in which the electromagnetic acceleration is dominant. The pressure term relevant to the aerodynamic effect is duely dropped. The energy equation will not be involved in the governing equations from this assumption as well as the third assumption. The fifth assumption is realistic since the plasma is highly ionized except near the gas inlet and the conductivity is rather insensitive to the plasma density in accordance with Spitzer's formula.[5] The conductivity is a function of electron temperature which, in general, is uniform in the arc discharge.

The fundamental equations are as follows in the coordinate system shown in Fig. 2.

Mass conservation

$$\rho u A = \dot{m} \tag{1}$$

Equation of motion

$$\rho u \frac{\mathrm{d}u}{\mathrm{d}x} = jB_z \tag{2}$$

Induction equation

$$j = -(1/\mu)\frac{\mathrm{d}B_z}{\mathrm{d}x} \tag{3}$$

Ohm's law

$$j = \sigma[(V/A) - uB_z] \tag{4}$$

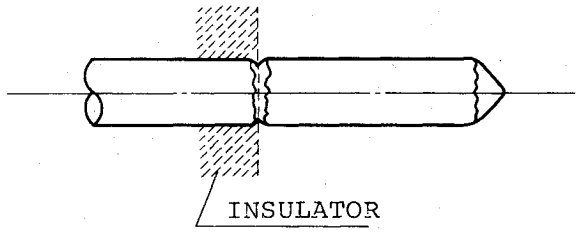

Fig. 1 Erosion near cathode root.

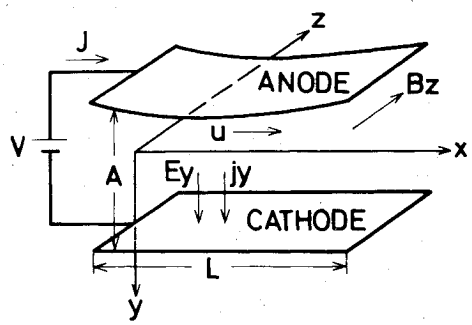

Fig. 2 Quasi-one-dimensional electrode system.

Where ρ is the density, $\dot{m}$ the mass flow rate per unit transverse length, j the current density, B_z the z component magnetic flux, and V the voltage applied between electrodes. The plasma velocity has only an x component u. The electrode separation A is a function of x. The origin of the coordinate system is taken at the entrance of the accelerator and the streamwise electrode length is L. The energy equation comes into play when the thrust efficiency is calculated from the solutions of Eqs. (1-4). Since the aerodynamic effect is ignored, as stated earlier, the Joule heating is not treated to be fed back to the enthalpy but to be simply wasted. The boundary conditions are

$$u=0 \text{ at } x=0, \qquad B_z=0 \text{ at } x=L \tag{5}$$

The latter condition is the requirement that the discharge current should terminate at the channel exit.

The variables are nondimensionalized as ξ, b, v, and δ, which are given by

$$x=L\xi, \quad B_z=B_0 b, \quad u=\hat{A}B_0^2 v/2\mu\dot{m}, \quad A=\hat{A}\delta(\xi) \tag{6}$$

where B_0 is the magnetic flux at the entrance of the channel, and

$$\hat{A}=\int_0^1 A\,\mathrm{d}\xi \tag{7}$$

By means of these variables the fundamental equations are nondimensionalized. From Eqs. (1), (2), and (4),

$$\frac{\mathrm{d}v}{\mathrm{d}\xi}=2Rm\delta\left(\frac{\phi}{\delta}-\frac{vb}{2}\right)b \tag{8}$$

is derived, and from Eqs. (3) and (4)

$$\frac{\mathrm{d}b}{\mathrm{d}\xi}=-Rm\left(\frac{\phi}{\delta}-\frac{vb}{2}\right) \tag{9}$$

is derived, where

$$Rm=\sigma B_0^2 L\hat{A}/\dot{m}, \qquad \phi=\mu V\dot{m}/B_0^3\hat{A}^2 \tag{10}$$

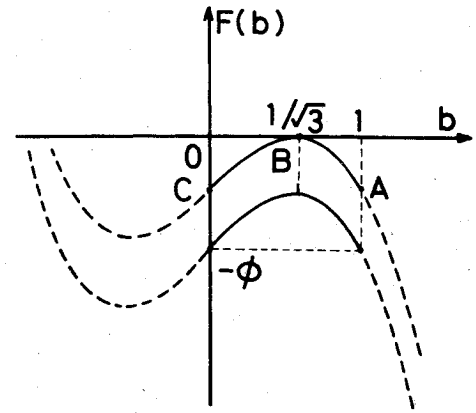

Fig. 3 Parametric dependence of $F(b;\phi)$.

Here Rm represents the magnetic Reynolds number with reference to the velocity $B_0^2\hat{A}/\mu\dot{m}$, which is roughly proportional to the exit velocity. Since the magnetic flux B_0 is expressed in terms of the discharge current per unit span J

$$B_0=\mu J \tag{11}$$

Rm is the parameter representing $J^2/\dot{m}$. The parameter ϕ is representing the discharge voltage. The boundary conditions in the nondimensional form are given by the equations

$$b=1,\ v=0 \text{ at } \xi=0, \qquad b=0 \text{ at } \xi=1 \tag{12}$$

As the discharge parameter, one can specify either the current parameter Rm or the voltage parameter ϕ. Suppose Rm is specified, Eqs. (8) and (9) are integrated with the boundary conditions specified at $\xi=0$ and ϕ assumed. If $b=0$ is not satisfied at $\xi=1$ as result of integration, ϕ is revised and the integration process is repeated until the boundary condition at $\xi=1$ is fulfilled. The set of Rm and ϕ thus obtained is the voltage-current characteristics of the discharge.

In order to foresee the general characteristics of Eqs. (8) and (9), and simplest case, $A=\text{const}$ or $\delta(\xi)\equiv 1$, is considered. With Eqs. (8) and (9) combined, an integration results.

$$v=1-b^2 \tag{13}$$

Inserting this result into Eq. (9), a first-order differential equation is obtained.

$$\frac{1}{Rm}\left(\frac{\mathrm{d}b}{\mathrm{d}\xi}\right)=-\{\phi-(1-b^2)b/2\} \equiv F(b;\phi) \tag{14}$$

When b is solved from this equation, v is found by means of Eq. (13). The right-hand side of Eq. (14), $F(b)$, is schematically drawn in Fig. 3. The curve has a physical meaning in the region $0<b<1$ as represented by the solid line. As ϕ is reduced, the maximum point B in this figure shifts upward until it touches the b axis. In this limit, the integration starting from point A cannot proceed beyond B, where $\mathrm{d}b/\mathrm{d}\xi=0$ and $b=1/\sqrt{3}$. This singularity is associated with the limit $Rm\to\infty$. Since the left-hand side diminishes in the limit $Rm\to\infty$, Eq. (14) has a meaning only in the boundary regions at $\xi=0$ and $\xi=1$ whose thicknesses are $O(Rm^{-1})$ as shown in Fig. 4. Between the two boundary regions, the core region or zero current region appears, which is degenerated into the

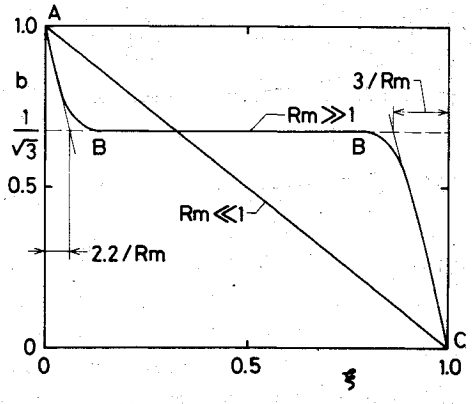

Fig. 4 Schematics of inlet and outlet boundary regions. Points A, B, and C correspond to those in Fig. 3.

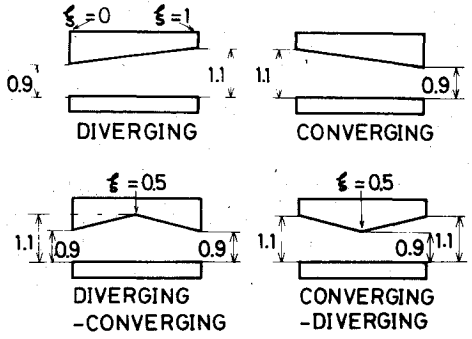

Fig. 5 Electrode configurations. Channel width is expressed in terms of $\delta(\xi)$ defined by Eqs. (6) and (7).

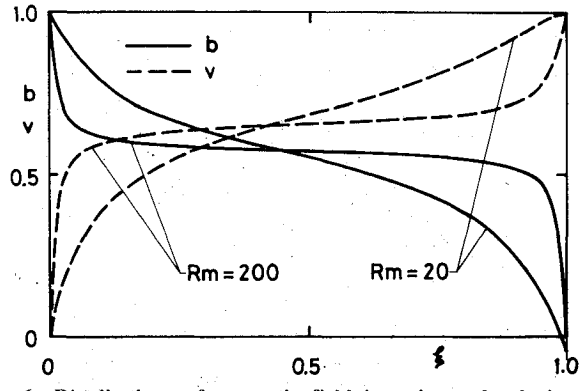

Fig. 6 Distributions of magnetic field intensity and velocity for straight electrode.

point B in Fig. 3. In this limiting condition, the thrust efficiency defined as

$$\eta = \dot{m}u_L^2/2VJ = v(1)^2/8\phi \tag{15}$$

takes a maximum value $3\sqrt{3}/8$, where u_L is the exit velocity.

Results and Discussion

Equations (8) and (9) are solved for the electrode geometries such as diverging (D), converging (C), diverging-converging (DC), and converging-diverging (CD) types shown in Fig. 5, in addition to straight (S) type or parallel flat plates discussed in the last section.

The numerical calculations were made specifying the current parameter Rm. In Fig. 6 the streamwise variation of magnetic field b and velocity v is shown for S type. The distribution of current density normalized by the value at $\xi = 0$ is depicted in Fig. 7 also for S type. As Rm is increased, the

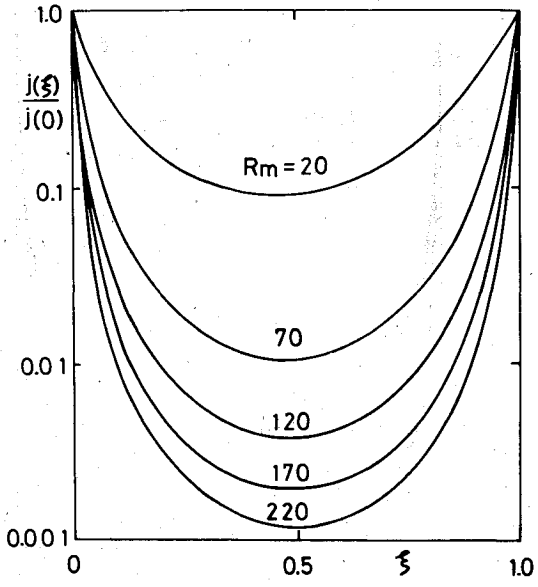

Fig. 7 Distribution of current density for straight electrode.

discharge current is concentrated at the entrance $\xi = 0$ and the exit $\xi = 1$. This feature, if applied to the MPD arcjet, implies that the current concentration and, hence, the concentrated power loading occur at the electrode root and tip. Since the thickness of the boundary region at $\xi = 0$ and $\xi = 1$ is $O(Rm^{-1})$ in nondimensional form, the current density in this region is estimated to be

$$j = cJRm/L = c\sigma\mu^2 J^3 \hat{A}/\dot{m} \tag{16}$$

where c is a constant factor of about 0.2 as obtained from Fig. 4. When this value exceed the critical value j_{cr} depending on the electrode material, 10^4-10^5 A/cm^2, cathode and anode spots are formed and the detrimental erosion starts.[6,7] Therefore, the condition

$$j_{cr} \geq c\sigma\mu^2 J^3 \hat{A}/\dot{m} \tag{17}$$

is prerequisite for the erosion free operation of the accelerator. Equation (17) involves the averaged electrode separation $\hat{A}$ and gives a limitation to the accelerator scale.

It is shown in Figs. 6 and 7 that little current is flowing between the central parts of electrodes. This result suggests modification of the electrode geometry in such a manner that the separation is smaller at the middle of electrodes. This is the motivation to study CD type electrodes. Other geometries are also studied for comparison. The nondimensional current density $-db/d\xi$ is shown in Fig. 8 for S, D, C, and CD types at $Rm = 220$. The D, C, and CD types are found to have more uniform distribution than the S type at large Rm. The small difference in $-db/d\xi$ among these geometries is attributable to the small variation of $\delta(\xi)$. In order to reserve the quasi-one-dimensionality, the variation of δ is restricted to be within 10%. If a larger amplitude is admitted for δ, a more uniform distribution may result, especially for the CD type. In Fig. 9, the distribution of magnetic flux b and velocity v is shown for the DC type. The situation becomes worse than the S type with respect to the current concentration at both ends of the electrode. Furthermore, the direction of current is reversed in the region $0.15 \leq \xi \leq 0.5$. This implies that a current vortex is formed in the plasma via electrodes. The current reversal was observed at Rm as low as 30 and was not found at and below $Rm = 20$. In the region of current reversal the plasma feeds back the power to the power supply and, therefore, the flow is decelerated.

The thrust efficiency is determined by the combined effect of $v(1)$ and ϕ as found in Eq. (15). The nondimensional

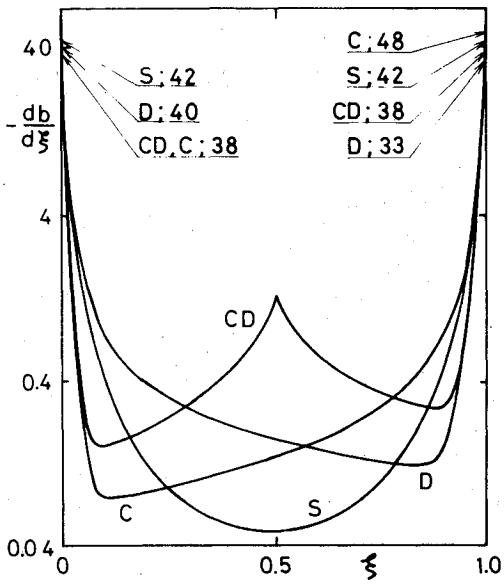

Fig. 8 Distribution of current density, $-db/d\xi$ for various electrode configurations: S, straight; D, diverging; C, converging; CD, converging-diverging; $Rm = 220$.

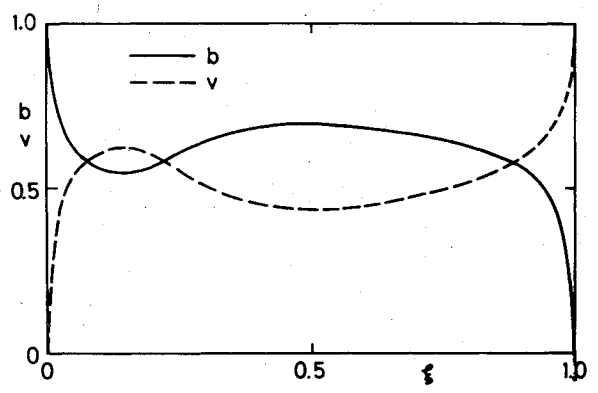

Fig. 9 Distribution of magnetic field intensity and velocity for diverging-converging electrode; $Rm = 200$.

exhaust velocity $v(1)$ is shown as a function of Rm in Fig. 10. From Eq. (13) $v(1) = 1$ results for S type. For D type $v(1)$ is 5% less than S type and 10% less for DC type. The CD type has the largest $v(1)$ in all the geometries. Figure 11 illustrates the variation of the voltage parameter ϕ with Rm. As discussed in the last section, ϕ for S type decreases asymptotically to $1/3\sqrt{3}$ as Rm is increased. As in other cases, ϕ curves have asymptotes as $Rm \to \infty$. The limiting values for D and DC types are 10% smaller than S type. From these $v(1)$ and ϕ results, the thrust efficiency was calculated and is plotted against Rm in Fig. 12. The S type has a maximum limiting value $3\sqrt{3}/8$ as stated earlier. The CD type has the highest thrust efficiency in the various electrode geometries studied so far. The high efficiency results from the large exhaust velocity and the low voltage as found in Figs. 10 and 11, respectively. When the efficiency was calculated by shifting the throat location upstream and downstream, the results were found to be hardly affected unless the position was close to $\xi = 0$ or $\xi = 1$. The DC type has the lowest efficiency. In this case the acceleration is inefficient due to the reversed current as shown in Fig. 9, and the exhaust speed is comparatively low. This is the cause of the low thrust efficiency of the DC type. In conclusion, although the distributions of current density for various electrode geometries indicate only slight differences, the resulting thrust efficiencies demonstrate 10% variation. It can be suggested from these discussions that the thrust efficiency is sensitive to the electrode geometry and the efficiency improvement is expected by an elaborate analysis taking into account the three-dimensional electrode geometry.

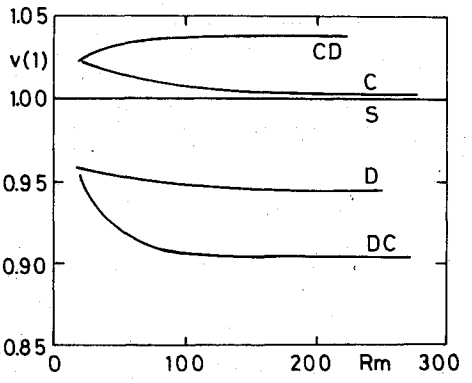

Fig. 10 Exhaust velocity for various electrode configurations, see Fig. 8 for notation.

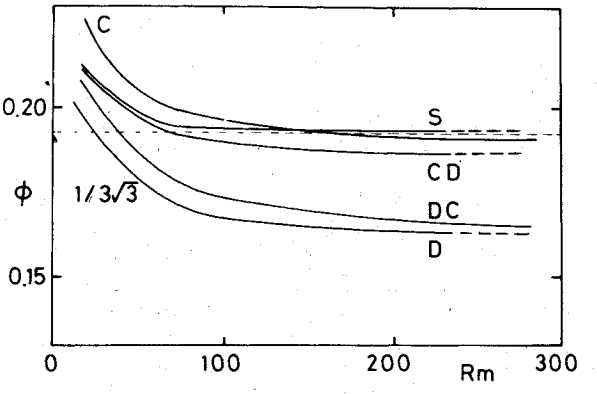

Fig. 11 Voltage parameter for various electrode configurations, see Fig. 8 for notation.

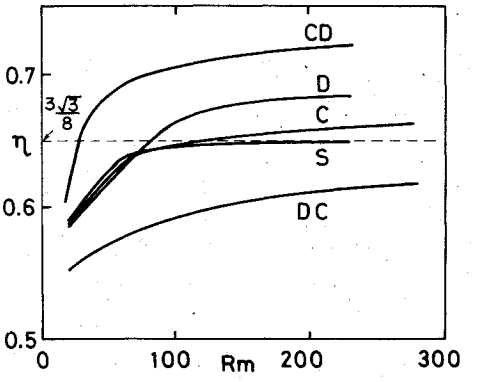

Fig. 12 Thrust efficiency for various electrode configurations, see Fig. 8 for notation.

As shown in Fig. 12, the efficiency does not tend to be 100% even if Rm becomes infinitely large. This result may well look peculiar if the Rm increase is regarded as the increase of σ and, hence, the decrease of Joule loss. To solve this contradiction, the efficiency is written as

$$\eta = P_A/(P_A + P_J) \tag{18}$$

where P_A and P_J represent the powers for acceleration and Joule heating, respectively. The power for acceleration is approximately given by

$$P_A = \int_0^{\delta_1} A\left(\frac{J}{\delta}\right) uB_z \mathrm{d}x + \int_{L-\delta_2}^{L} A\left(\frac{J}{\delta}\right) uB_z \mathrm{d}x \quad \propto J^4 \tag{19}$$

where the current is assumed to flow only in the inlet and exit boundary regions of respective thickness, δ_1 and δ_2. Likewise, the power for the Joule heating is given by

$$P_J = \int_0^{\delta_1} A(J^2/\delta^2\sigma)\,dx + \int_{L-\delta_2}^{L} A(J^2/\delta^2\sigma)\,dx$$

$$\propto J^2/\delta\sigma \text{ or } J^4 \qquad (20)$$

if the relation δ_1 and $\delta_2 \propto Rm^{-1}$ is taken into account. By inserting the last forms of Eqs. (19) and (20) into Eq. (18), one can find that the efficiency tends to be a constant less than unity as J increases. To sum up, the fractional power of Joule loss does not diminish due to the current concentration even when Rm is increased.

It may well be asked why, as conventionally admitted, the discharge current does not totally concentrate at the channel exit by blowoff effect of the flow. This effect of current convection explains one of the effects determining the current distribution. Another effect is the potential or static effect which dominates in the flow at low velocity. When Rm is small, the current distribution is dominated by the diffusion and the latter effect is dominant over the entire region. Therefore, the uniform current distribution results as shown in Fig. 4. When Rm is large, the current concentration by the static effect is significant only at the channel entrance. As soon as the flow is accelerated to the drift velocity $u=E/B_z$, no more current flows between electrodes, as shown in Fig. 4. Here E represents the electric field and $E=V/A$. The discharge current is convected downstream and concentrated at the channel exit. When the magnetic field distributions for small and large Rm are compared in Fig. 4, the magnetic flux is found to be conveyed from the upstream to downstream region in the large Rm case.

Conclusions

The magnetohydrodynamic analysis has been made on the quasi-one-dimensional self-field accelerator. The results are as follows.

1) Magnetic Reynolds number Rm was an essential non-dimensional parameter describing the current distribution.

2) As Rm is increased, the discharge current concentrates in boundary regions at the channel entrance and exit.

3) The thickness of the boundary region is inversely proportional to Rm and little current flows outside the boundary regions at high Rm.

4) The limitation on the accelerator scaling was derived.

5) The converging-diverging electrode configuration was found favorable to relax the current concentration and to have high thrust efficiency.

6) The diverging-converging electrode configuration has a reversed current from cathode to anode at high Rm, and was proved to be an inefficient configuration.

References

[1] Kuriki, K. and Suzuki, H., "Transitional Behavior of MPD Arcjet Operation," *AIAA Journal,* Vol. 16, Oct. 1978, pp. 1062-1067.

[2] Seals, R. K. Jr. and Hassan, H. A., "Analysis of MPD Arcs with Nonequilibrium Ionization," *AIAA Journal,* Vol. 6, Dec. 1968, pp. 2273-2278.

[3] Hügel, H., Maisenhälder, F., and Schock, W., "Investigations of Plasma Flows Accelerated by the Self-Magnetic Effect," AIAA Paper 70-1098, Aug.-Sept. 1970.

[4] Kimura, I., Toki, K., and Tanaka, M., "Current Distribution on the Electrodes of MPD Arcjets," AIAA Paper 81-0682, April 1981.

[5] Spitzer, L. Jr., *Physics of Fully Ionized Gases,* Interscience Publishers, 1962, Chap. 5.

[6] Lyubimov, G. A. and Rakhovskii, V. I., "The Cathode Spot of a Vacuum Arc," *Soviet Physics, Uspekhi,* Vol. 21, Aug. 1978, pp. 693-718.

[7] Miller, H. C., "Vacuum Arc Anode Phenomena," *IEEE Transactions on Plasma Science,* Vol. PS-5, Sept. 1977, pp. 181-196.